Cell cycle, apoptosis, cellular uptake and whole-transcriptome microarray gene expression analysis of HeLa cells treated with Ruthenium(II)-arene complex with isoquinoline-3-carboxylic acid as ligand

Katarina K. Jovanović[a,#], Miljana Tanić[a,d,#], Ivanka Ivanović[b], Nevenka Gligorijević[a], Biljana P. Dojčinović[c], Siniša Radulović[a,*]

[a] *Institute of Oncology and Radiology of Serbia, Pasterova 14, 11000 Belgrade, Serbia*

[b] *Faculty of Chemistry, University of Belgrade, Studentski trg 12-16, 11 000 Belgrade, Serbia*

[c] *Institute of Chemistry, Technology and Metallurgy, Centre of Chemistry, University of Belgrade, Studentski trg 12-16, Belgrade, Serbia*

[d] *Present address: UCL Cancer Institute, University College London, London, United Kingdom*

[#] *K.K. Jovanović and M. Tanić contributed equally to this work*

Abstract

Ruthenium(II)-arene complexes are promising drug candidates for the therapy of solid tumors. In our previous work, seven new ruthenium(II)-arene complexes of the general formula [Ru(η^6-*p*-cymene)(L^{1-7})Cl] were synthesized and characterized, of which the complex with L = isoquinoline-3-carboxylic acid (**RuT$_7$**), was two times as active on HeLa cells compared to normal cell line MRC-5, as indicated by IC50 values determined after 48 h of (45.4 ± 3.0) vs. (84.2 ± 5.7) μM, respectively.. In the present study, cell cycle analysis of HeLa cells treated with RuT$_7$ showed S phase arrest and an increase in the sub-G1 population. The apoptotic potential of investigated compound was confirmed with the Annexin V-FITC/PI assay together with a morphological evaluation of cells using fluorescent microscopy. Analysis of the intracellular accumulation of ruthenium showed the presence of metal inside the cells

* Address for correspondence: Institute of Oncology and Radiology of Serbia, Pasterova 14, 11000 Belgrade, Serbia, E-mail address: sinisar@ncrc.ac.rs. Tel: +381 11 2067 434. Fax: +381 11 2067 294

already after 6 h incubation period (8.90 ng Ru/10^6 cells). To gain further insight into the molecular mechanism of the biological action of **RuT$_7$** against HeLa cells, a whole-transcriptome microarray gene expression analysis was performed. Analysis of functional categories and signaling and biochemical pathways associated with response of HeLa cells to treatment with **RuT$_7$** complex showed that it leads the cells through the intrinsic (mitochondrial) apoptotic pathway,, via indirect DNA damage due to the action of reactive oxygen species, and through direct DNA binding of **RuT$_7$**. Statistical analysis for enrichment of gene sets associated with known drug-induced toxicities identified fewer associated toxicity profiles in **RuT$_7$** treated cells compared to cisplatin treatment. Altogether these results provide the basis for development of **RuT$_7$** in animal and pre-clinical studies as a potential drug candidate.

Keywords: ruthenium(II), anticancer drugs, apoptosis, HeLa, microarray

1. Introduction

Since the first success of cisplatin in cancer therapy numerous alternatives to this most widely used chemotherapeutic agent have been proposed. Although cisplatin and its analogues (carboplatin, oxaliplatin) have undoubtedly been proven to be highly effective against several types of epithelial cancer, including ovarian, bladder and testicular cancer, these drugs display only limited therapeutic activity against the most common tumors, such as colon and breast cancer [1]. Taking into account the limited scope of cisplatin treatment, coupled with the emergence of secondary tumor resistance and a range of dose-limiting adverse effects, such as nephrotoxicity, peripheral neurotoxicity and emetogenesis, there is an imminent need for the development and clinical introduction of alternative antineoplastic agents [2].

To overcome these issues, a large number of ruthenium-based compounds have been developed and tested in pre-clinical studies showing high anticancer activity and fewer associated toxicities compared to platinum-based drugs. Three ruthenium(III) compounds have shown high *in vitro* and *in vivo* antitumor activity and have managed to reach clinical trials: NAMI-A (trans-[tetrachlorido(1H-imidazole)(S-dimethyl sulfoxide) ruthenate(III)]), KP1019 (indazolium trans-[tetrachloridobis (1H-

indazole) ruthenate(III)]) and NKP1339 (sodium trans-[tetrachloridobis(1H-indazole) ruthenate(III)]) [3-6]. NAMI-A exhibited selective effect on metastases of solid tumors, with no effect on primary tumor growth, while KP1019 showed pronounced cytotoxic effect, especially in colorectal tumor cells and carcinomas [7-9].

Emerging *in vivo* data on two prototypical compounds, [Ru(η^6-*p*-cymene)Cl(en)], where en = ethylenediamine (RAED-C) and [Ru(η^6-*p*-cymene)Cl2(pta)], where pta = 1,3,5-triaza-7-phosphaadamantane (RAPTA-C), put the focus on ruthenium(II)-arene compounds. It is shown that, regardless the low *in vitro* activity, RAPTA-C is very active *in vivo*, where it inhibits lung metastases in CBA mice [10]. Besides supposed low general toxicity and high selectivity of ruthenium compounds for cancer cells, ruthenium(II)-arene complexes are characterized by hydrophobic arene ligand which is counterbalanced by the hydrophilic metal centre. These features, together with synthetic diversity of the arene ligand, make ruthenium(II)-arene compounds appealing candidates for anticancer drug design [11].

In our previous work we have reported synthesis and characterization of seven new ruthenium(II)-arene complexes [Ru(η^6-*p*-cymene)(L^{1-7})Cl], where L^{1-7} are fluoro, chloro, bromo or methyl derivatives of picolinic acid or isoquinoline-3-carboxylic acid [12]. DNA binding study have demonstrated DNA binding potential of [Ru(η^6-*p*-cymene)(L)Cl], where L = isoquinoline-3-carboxylic acid (**RuT$_7$**). Obtained increase in absorbance (hyperchromism) of calf thymus (CT) DNA reflects altered conformation of DNA double-helix via intercalation of investigated complex *in vitro* [13]. After preliminary screening of antiproliferative activity against tumor and normal cell lines, we have identified **RuT$_7$** complex as a promising drug candidate (**Figure 1**).

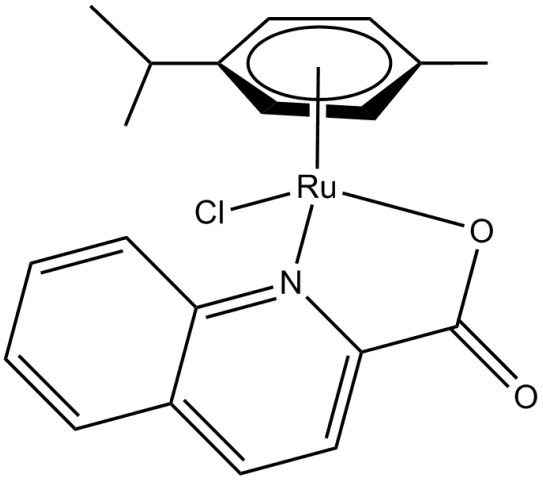

Figure 1. Structure of ruthenium(II)-arene complex **RuT7**, [Ru(η^6-*p*-cymene)(L)Cl]

Although many of the mechanisms of action of the ruthenium-based complexes are not yet fully understood, besides the inhibition of the metastases [14, 15], other mechanisms have been proposed as well, such as interactions with DNA [16], interactions with proteins [17], production of reactive oxygen species [18], inhibition of topoisomerase activity [19, 20], induction of apoptosis [21] and antiangiogenic effects [22, 23]. Recently, studies oriented towards elucidating molecular background underlying biological mechanisms of action of ruthenium-based complexes began to emerge. In a recent study, Bergamo et al. performed whole-transcriptome analysis and RNA-sequencing of the metastatic MDA-MB-231 mammary carcinoma and non-tumorigenic HBL-100 mammary gland cells, treated with antimetastatic agent NAMI-A, demonstrating a differential response between MDA-MB-231 and HBL-100 cells to NAMI-A treatment, at the level of cell cycle regulation and ECM (extracellular matrix) remodeling in MDA-MB-231 cells [24]. In another work, a genome profiling of the human ovarian and cisplatin-resistant human ovarian cancer cell lines (A2780 and A2780cisR) treated with hydrazinyl-thiazolo arene ruthenium complexes has been performed. The results have shown that these compounds lead both cancer cell lines through apoptotic and cell death-related processes via p53 signaling pathway, despite the fact that signal transduction occurs through different molecules in these cell lines [25]. Although still very sparse, studies regarding molecular mechanisms of ruthenium compounds action are of great importance for providing valuable information for successful compound design.

In this study we have performed a comprehensive analysis of both cellular and molecular response to **RuT$_7$** treatment on HeLa cells. To elucidate the mode of action of **RuT$_7$** complex, gene expression profiling using Whole Human Genome Agilent array technology was applied and the whole transcriptome analysis was performed. We have identified gene expression perturbations, associated pathways and molecular functions induced by **RuT$_7$** complex treatment of HeLa cells. Additionally, we have assessed *in silico* the potential drug sensitivity and toxicity effects of **RuT$_7$** complex in comparison to cisplatin treatment. Therefore, the main objectives of this study were to identify significantly enriched biological functions and canonical pathways as a result of drug treatment at 12 h and 24 h time points, to identify gene clusters whose expression changes over the time (time-course) and to identify differences in predicted toxicity profiles between cells treated with **RuT$_7$** complex and cisplatin.

2. Materials and Methods

2.1 Cell lines and culture conditions

The human cervical carcinoma (HeLa) cells were maintained as a monolayer culture in the Roswell Park Memorial Institute (RPMI) 1640 nutrient medium (Sigma Chemicals Co, USA). RPMI 1640 nutrient medium was prepared in sterile deionised water, supplemented with penicillin (192 IU/mL), streptomycin (200 µg/mL), 4-(2-hydroxyethyl) piperazine-1-ethanesulfonic acid (HEPES) (25 mM), L-glutamine (3 mM), and 10% of heat-inactivated fetal calf serum (FCS) (pH 7.2). The HeLa cells were grown at 37 °C in 5% CO_2 in a humidified air atmosphere.

2.2 Cell cycle analysis

Flow-cytometric analysis of the cell cycle phase distribution of HeLa cells, treated with investigated ruthenium complex and CDDP as reference compound was performed after staining fixed HeLa cells with propidium iodide (PI) [26].

HeLa cells were seeded at a density of 2 x 10^5 cells/well, in 6-well plates (NUNC), and grown in complete nutrition medium. After 24 h, the cells were continually exposed to tested compound and

CDDP with concentrations that correspond to 0.5 x IC_{50} and IC_{50} (previously determined for 48 h treatment [12]). After 24 and 48 h of continual treatment, the cells were collected by trypsinization, washed twice with ice-cold PBS, and fixed for 30 min in 70% EtOH. After fixation, the cells were washed again with PBS, incubated with RNaseA (1 mg/mL) for 30 min at 37 °C and stained with PI (400 μg/mL) 15 min before flow-cytometric analysis. Cell cycle phase distribution was analyzed using a fluorescence activated sorting cells (FASC) Calibur Becton Dickinson flow cytometer and the Cell Quest computer software.

2.3 Apoptotic assay

Induction of apoptosis by **RuT$_7$** complex and CDDP in HeLa cells was evaluated by Annexin V–FITC apoptosis detection kit (BD Biosciences Cat. No. 65874x, Pharmingen San Diego, CA, USA). Briefly, 1 x 10^6 HeLa cells/mL were treated with 0.5 x IC_{50} and IC_{50} concentrations of **RuT$_7$** complex and CDDP for 24 h. After treatment the cells were washed twice with cold PBS and then resuspended in 200 μL binding buffer (10 mM HEPES/NaOH pH 7.4, 140 mM NaCl, 2.5 mM $CaCl_2$). 100 μL of the solution (1 x 10^5 cells) was transferred to a 5 mL culture tube and 2.5 μL of Annexin V–FITC and 2.5 μL of PI were added. The cells were gently vortexed and incubated for 15 min at 25 °C in the dark. Next, 400 μL of binding buffer was added to each tube and then analyzed using a FACS Calibur Becton Dickinson flow cytometer and the Cell Quest Pro computer software.

2.4 Morphological evaluation of HeLa cell death

To examine the mode of HeLa cell death induced by the investigated compound, morphological analysis by microscopic examination of acridine orange/ethidium bromide-stained target cells was performed. HeLa cells were seeded overnight on coverslips in 6-well plates (1.5 x 10^5 cells per well) in 2 mL of complete nutrient medium. After 24 h, the cells were treated with investigated ruthenium compound for 1, 3, 5 and 24 h at concentrations corresponding to 0.5 x IC_{50} values that were obtained after treatments that lasted 48 h. After this period, the target cells were stained with 10 μL of a mixture of the DNA dyes acridine orange and ethidium bromide (3 mg/mL AO and 10 mg/mL EB in PBS), and

visualized under a fluorescence microscope – Carl Zeiss PALM MicroBeam with Axio Observer.Z1 using AxioCam MRm (filters Alexa Fluor 489 and Alexa Fluor 546) using the Fluar 10x/0.30 M27 and LD Plan-NeoFluar 40x/0.60 Corr Ph2 M27 objectives. Images were obtained with multidimensional acquisition using digital imaging software (AxioVision Version 4.7; Carl Zeiss Imaging Solutions).

2.5 Inductively coupled plasma mass spectrometry (ICP-MS)

Ru accumulation was analyzed in HeLa cells with inductively coupled plasma mass spectrometry (ICP-MS) using Thermo Scientific iCAP Qc ICP-MS (Thermo Scientific, Bremen, Germany) [27]. HeLa cells were seeded at 1 x 10^6, 0.7 x 10^6 and 0.5 x 10^6 densities in a 25 cm^2 falcon dish (Thermo Scientific Nunc™) for 6, 24 and 48 h treatment, respectively. After 24 h stabilization period, the cells were treated with the **RuT$_7$** complex at concentration equal to 1 x IC_{50}. Following 6, 24 and 48 h, the cells were harvested by scraping, washed by ice cold PBS and the cell pellet was collected by centrifugation at 2000 rpm, 10 min.

2.6 HeLa treatment and RNA extraction protocol

HeLa cells were seeded in triplicate, at 1 x 10^6 and 0.7 x 10^6 densities in a 25 cm^2 falcon dish (Thermo Scientific Nunc™) for 12 and 24 h treatment, respectively. At 24 h after seeding, the cells were treated with 0.5 x IC_{50} concentrations of **RuT$_7$** complex, CDDP, or left untreated as control. Following 12 and 24 h, the cells were harvested and total RNA was extracted using the Trizol reagent (Invitrogen), and purified using the RNeasy Mini Kit (QIAGEN). RNA quantity and quality was estimated using the BioSpec Nano spectrophotometer (Shimadzu Scientific Instruments) and 1% agarose gel electrophoresis.

2.7 Microarray hybridization procedure

Briefly, 100 ng of total RNA per sample was labeled with Cy3 fluorescent dye using the Low Input Quick Amp Labeling Kit (Agilent Technologies, Santa Clara, CA, USA) and subsequently hybridized over 17 h at 65ºC onto an Agilent SurePrint G3 Hmn GE 8x60 K microarray, covering

27958 Entrez genes and 7419 lncRNAs. Each sample was hybridized in triplicate for each condition (control, **RuT**$_7$ and CDDP) at each time point (12 h and 24 h), for a total of 18 samples. Detailed description of procedures for sample labeling and microarray hybridization is in Supplementary Methods.

2.8 Microarray data pre-processing and data analysis

Processed slides were scanned with the Agilent SureScan Microarray Scanner (Agilent Technologies) and images were processed using the Agilent Feature Extraction v.11 software (Agilent Technologies). Quality Control report was used to evaluate the reliability and reproducibility of each microarray, and 2 samples were discarded from further analysis. Microarray data pre-processing and differential expression analysis was performed using the GeneSpring v.13.1 software (Agilent Technologies). In brief, flagged probes and control probes were filtered out, raw intensity values were averaged over the replicate probes, and background corrected data was normalized by scaling to 75th percentile and log 2 transformed. Additionally, sample quality control was performed by principal component analysis and 3 outlier samples were excluded from further downstream analysis. Microarray dataset is publicly available at the GEO database (http://www.ncbi.nlm.nih.gov/geo/info/linking.html) under GSE72905 accession number.

A moderated t-test was applied to identify differentially expressed genes between treatment conditions, and the estimated significance levels (unadjusted p-values) were corrected for multiple hypotheses testing using Benjamini and Hochberg false discovery rate (FDR) adjustment [28]. Genes with less than 0.05 false discovery rate (q-value) and greater than 2-fold differences in expression between the groups were considered to be significantly differentially expressed.

Supervised clustering analysis, applying average linkage method and Pearson uncentered correlation coefficient, was performed using the Cluster 3.0 software [29] and visualized using the JavaTreeView (http://jtreeview.sourceforge.net).

Time-course analysis of gene expression changes between different conditions was performed using the MaSigPro algorithm implemented within the Babelomics 4.0 bioinformatics suite

(http://babelomics.bioinfo.cipf.es/), applying a two-step multivariate linear regression model [30, 31]. Trajectory plots were used to visualize the results as time-dependent changes of gene expression between control and treated cells. Details of the analysis are described in the Supplementary Methods.

2.9 Gene set enrichment analysis and functional annotation

Ingenuity Pathway Analysis software (http://www.ingenuity.com) was used to identify pathways or biological functions with statisticaly significant over-representation in a given gene list, by applying the Fisher exact test [Hung JH et al. Gene Set/Pathway enrichment analysis. Methods Mol Biol. 2013]. All P values were corrected for multiple testing by Benjamini and Hochberg false discovery rate (FDR) adjustment; significance threshold was set to 0.05 FDR. IPA Core Analysis was performed to identify canonical signaling pathways, biological processes and gene networks significantly associated with drug-induced changes in gene expression for each treatment and time point. IPA Core Comparison analysis was performed to identify differences in enriched pathways between treatment-time points. Finally, IPA Tox Analysis was used to identify molecule-to-phenotype associations for know toxicities significantly enriched in the differentially expressed gene list for each of the compounds at 12 h and 24 h time points. All IPA analyses are described in detail in Supplementary Methods.

We have applied GOEAST - Gene Ontology Enrichment Analysis Software Toolkit [32] to identify significantly enriched gene ontology terms (GO) among the lists of genes belonging to specific Clusters, by inspecting both top significant GO terms and significant higher level GO functions. GO Term enrichment was calculated using hypergeometric probability distribution and the p-values were adjusted for multiple testing by controlling the false discovery rate (FDR) applying the Benjamini–Hochberg–Yekutieli procedure [33]. The significance threshold was set to 0.01 FDR.

3. Results

3.1 Cell cycle analysis

The effect of investigated ruthenium(II)-arene complex and CDDP on cell cycle progression of HeLa cells was examined by flow cytometry after continual treatment for 24 and 48 h, using staining with PI. HeLa cells were exposed to 0.5 x IC_{50} and 1 x IC_{50} concentrations of **RuT$_7$** and CDDP.

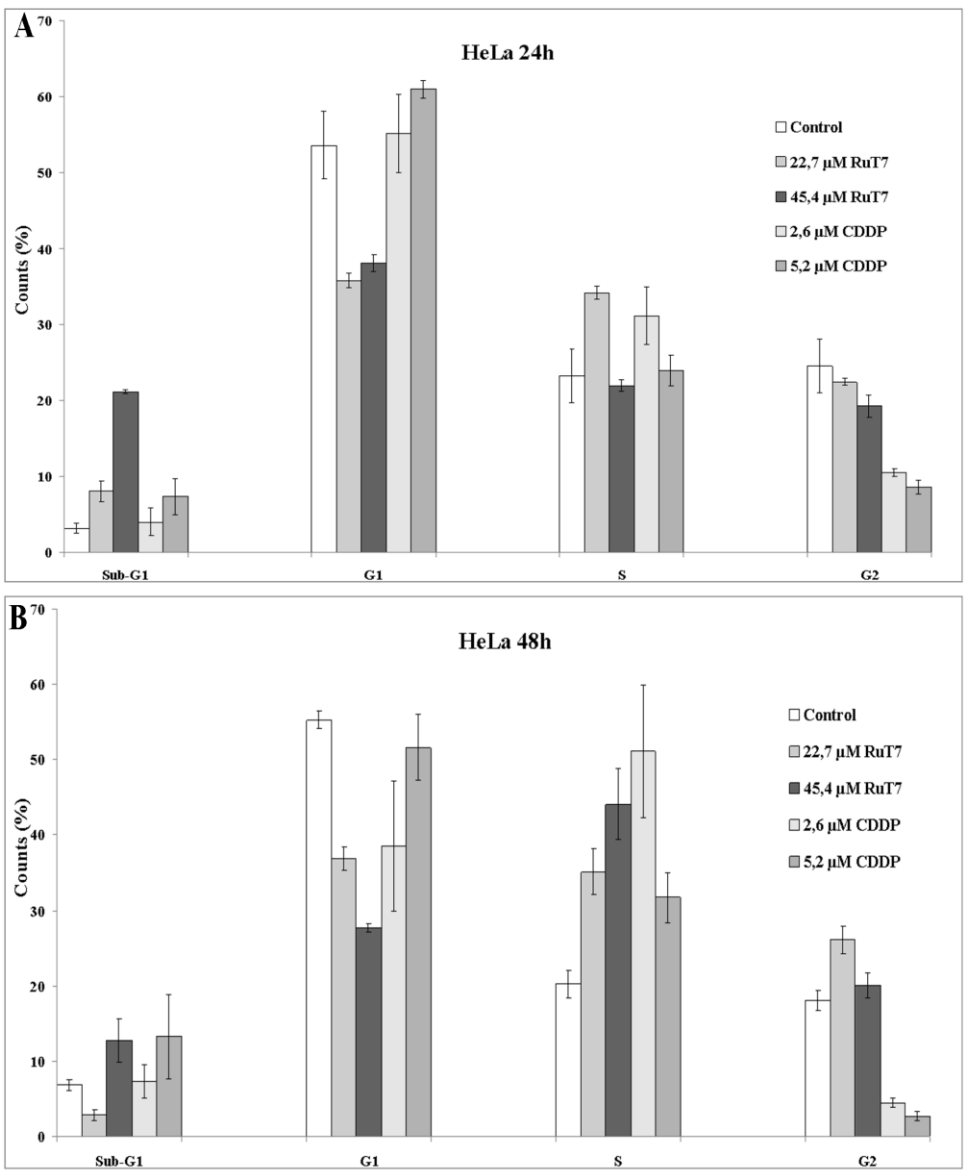

Figure 2. Effects of **RuT$_7$** and CDDP on cell cycle distribution. Untreated (control) HeLa cells or HeLa cells treated for 24 h (A) and 48 h (B) with 0.5 x IC_{50} and IC_{50} concentrations of **RuT$_7$** (22.7 and 45.4 µM) and CDDP (2.6 and 5.2 µM), respectively. The results are expressed as mean ± standard deviations of three independent experiments.

Following 24 h treatment with **RuT$_7$**, as shown in the Figure 2A, we observed a dose-dependent increase in sub-G1 population of cells with fragmented DNA(up to 20% with IC_{50}) compared to control (5%), and CDDP-treated cells (up to 8%)/ , with a corresponding decrease in the fraction of cells in the G1 phase compared to control cellswith both concentrations applied. Interestingly, there was an accumulation of both **RuT$_7$ and** CDDP-treatedcells in S phase with 0.5 x IC_{50} concentration applied (8% and XX compared to control, respectively), that was abrogated at higher concentrations. Moreover, in contrast to a more than 2-fold reduction of percent of cells in G2 phase , caused by CDDP treatment compared to control in both concentrations applied,, significantly larger number of cells manages to enter the G2 phase after **RuT$_7$** treatment.

After 48 h, differences in cell-cycle distribution profile between RuT_7 and CDDP-treated HeLa cells were further accentuated (Figure 2B).. On prolonged exposure of HeLa cells to **RuT$_7$**, the sub-G1 apoptotic peak decreased to 14% at 1xIC_{50}, in addition to further decrease in the fraction of cells in G1 phase (down to to 27% compared to control population) This was accompanied by an accentuated accumulation of cells in S phase, which was positively correlated to the RuT_7 concentration increase (35% and 43%, respectively), Notably, in RuT_7 treated cells G2/M fraction of cell was only slightly increased, in sharp contrast to depleted G2/M population of cells treated by CDDP.

3.2 Apoptotic assay

Potential of **RuT$_7$** and CDDP to induce apoptotic cell death was determined by staining treated HeLa cells with two dyes, Annexin V–FITC and propidium iodide, and analysis on flow cytometer.

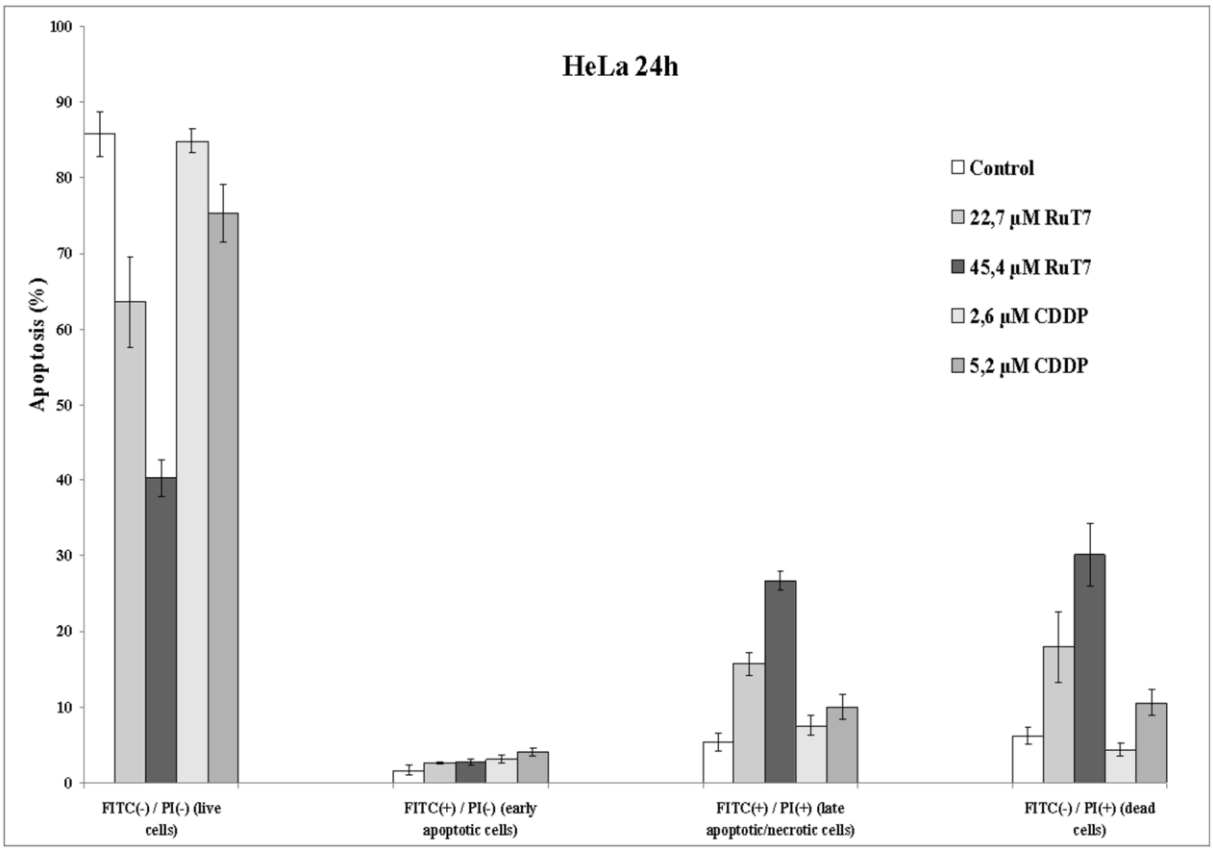

Figure 3. Apoptosis induction potential of **RuT$_7$** and CDDP. A. Cells were treated for 24 h with 0.5 x IC_{50} and IC_{50} concentrations of **RuT$_7$** (22.7 and 45.4 µM) and CDDP (2.6 and 5.2 µM), respectively; FITC(-)/PI(-) are live cells, FITC(+)/PI(-) are early apoptotic cells, FITC(+)/PI(+) are late apoptotic or necrotic cells and FITC(-)/PI(+) are dead cells. The results are expressed as mean ± standard deviations of three independent experiments

Results exhibited after 24 h exposure of HeLa cells to **RuT$_7$** reveal an increased number of cells in FITC(+)/PI(+) and FITC(-)/PI(+) subpopulations (**Figure 3**). At the same time, number of living cells with intact membranes that exclude both markers (FITC(-)/PI(-)) decreases, even more drastically with the increase of concentration of **RuT$_7$**. Treatment with CDDP in same experimental conditions did not manage to induce prominent effects on HeLa cells for this incubation period.

3.3 Morphological evaluation of HeLa cell death

In order to confirm apoptotic potential of investigated complex, morphological analysis by fluorescence microscopy of acridine orange/ethidium bromide-stained HeLa cells exposed for 1 - 24 h to **RuT$_7$** (0.5 x IC_{50} concentration) were performed.

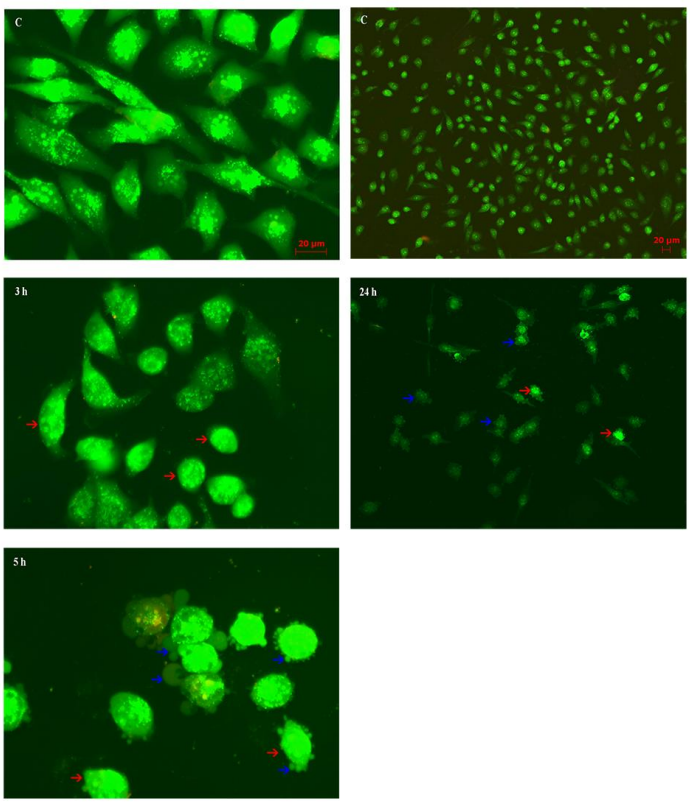

Figure 4. Photomicrographs of acridine orange/ethidium bromide-stained control (C) HeLa cells and HeLa cells exposed for 3 and 5 h to complex **RuT$_7$** (left), and photomicrographs of acridine orange/ethidium bromide-stained control (C) HeLa cells and HeLa cells exposed for 24 h to complex **RuT$_7$** (right). Red arrows point to cytoplasmic shrinkage and nuclear condensation; blue arrows denote membrane blebbing structures. Scale bars in the upper images correspond to magnification of photomicrographs below. Applied concentrations of **RuT$_7$** corresponded to 22.7 µM (0.5 x IC_{50}) values determined for 48 h incubation period

Control HeLa cells presented on photomicrographs in **Figure 4** are light green color, elongated and spindle-shaped. Already 3 h after treatment with **RuT$_7$** reduction in cell number is obvious; cells lose their normal morphology and became rounded. Early apoptotic markers such as cytoplasmic

shrinkage and nuclear condensation are present after **RuT$_7$** treatment. The most prominent morphological feature in **Figure 4** is membrane blebbing 5 h after treatment, which is unambiguous hallmark of apoptosis. Furthermore, after 24 h of treatment with ruthenium(II) complex, remaining adhered cells still undergo apoptosis, with aforementioned morphological features.

3.4 Intracellular accumulation of investigated RuT$_7$ complex

Total intracellular accumulation of investigated **RuT$_7$** complex after 6, 24 and 48 h treatment with 1 x IC_{50} concentration was analyzed using ICP-MS analysis [27].

Results on **Figure 5** show that ruthenium was found intracellular already 6 h after treatment (8.90 ng Ru/10^6 cells). The level of ruthenium was held stable with minor drop after 24 h continual treatment (7.09 ng Ru/10^6 cells). At 48 h time point ruthenium intracellular accumulation notably increases (11.92 ng Ru/10^6 cells). These results indicate long-term retention of ruthenium metal inside tumor cells.

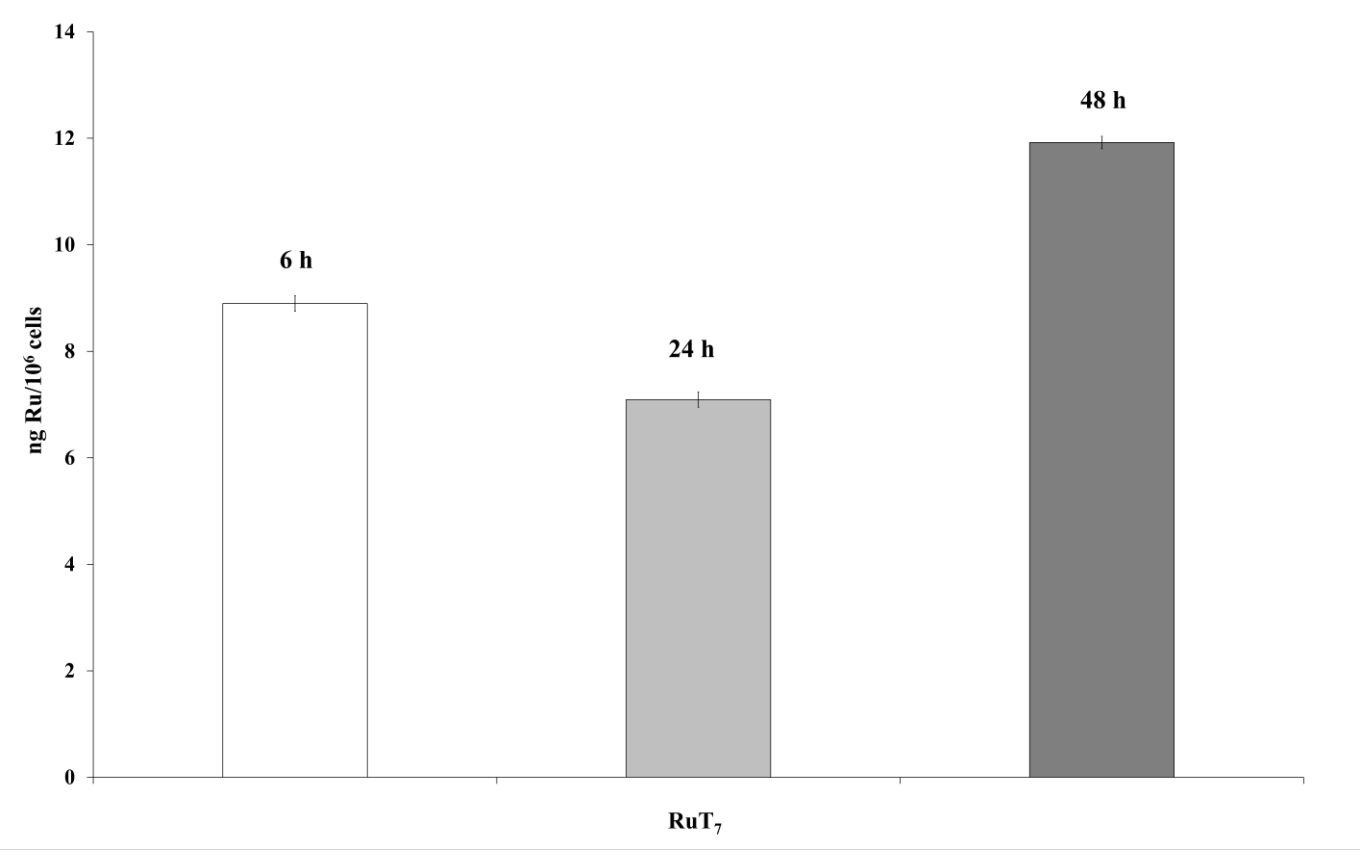

Figure 5. Total intracellular accumulation of ruthenium in HeLa cells after 6, 24 and 48 h, measured by ICP-MS. All experiments were performed in triplicate and presented with corresponding standard deviations (SD).

3.5 Differences in gene expression response to cisplatin and RuT$_7$ treatment in HeLa cells

We tested the effect of ruthenium(II)-arene of general formula [Ru(η^6-*p*-cymene)(L^7)Cl] (**RuT$_7$**) on HeLa cell line gene expression profiles at two time points, 12 and 24 h (**Figure 6A)**. The changes in gene expression induced by **RuT$_7$** complex were compared to HeLa cells treated with cisplatin (CDDP) at both time points. To identify significantly differentially expressed genes (DEG) induced by treatment with **RuT$_7$** complex or CDDP relative to control (untreated) cells at both time points, we performed moderated limma t-test (**Supplementary Table 1-4**). Treatment with **RuT$_7$** resulted in more subtle gene expression perturbation compared to the changes induced by CDDP treatment at both time points (**Figure 6B**). Treatment with **RuT$_7$** induced significant expression changes at 12 h compared to control cells in 2415 unique annotated genes, with 1184 upregulated and 1243 downregulated genes. The effect was potentiated at 24 h, with a total of 5988 DEG, of which 5475 were upregulated and only 545 downregulated. Top 20 significantly differentially expressed genes in response to **RuT$_7$** are shown in Table 1.

Table 1. Top-20 significantly differentially genes in **RuT$_7$** treated cells compared to control cells

Gene	Description	Unadjusted p-value	False Discovery Rate, FDR (q-value)	Fold Change	
12 h treatment					
LAT2	Linker for activation of T cells family, member 2	2.4E-07	3.2E-03	26.6	↑
OTOA	Otoancorin	3.0E-07	3.2E-03	33.6	↑
FBXW10	F-box and WD repeat domain containing 10	1.7E-07	3.2E-03	36.9	↑
BRD8	Bromodomain containing 8	1.8E-07	3.2E-03	43.1	↑
FOXD4	Forkhead box D4	5.5E-07	3.9E-03	19.0	↑
MYH3	Myosin, heavy chain 3, skeletal muscle,	5.2E-07	3.9E-03	20.0	↑
SV2B	Synaptic vesicle glycoprotein 2B	2.4E-06	4.3E-03	-10.0	↓
EDN2	Endothelin 2	2.5E-06	4.3E-03	-10.0	↓
COL9A3	Collagen, type IX, alpha 3	2.5E-06	4.3E-03	-7.5	↓
C11orf86	Chromosome 11 open reading frame 86	2.2E-06	4.3E-03	-6.7	↓
LOC91450	Uncharacterized LOC91450	2.5E-06	4.3E-03	6.8	↑
PLAC8L1	PLAC8-like 1	2.1E-06	4.3E-03	7.0	↑
VWCE	Von Willebrand factor C and EGF domains	2.6E-06	4.3E-03	7.2	↑
RNF151	Ring finger protein 151	2.9E-06	4.3E-03	8.0	↑
ELMO3	Engulfment and cell motility 3	3.0E-06	4.3E-03	8.6	↑
AOC3	Amine oxidase, copper containing 3	1.4E-06	4.3E-03	8.8	↑
CARD9	Caspase recruitment domain family, member 9	1.4E-06	4.3E-03	9.1	↑
C17orf51	Chromosome 17 open reading frame 51	2.3E-06	4.3E-03	9.3	↑
IFFO1	Intermediate filament family orphan 1	9.6E-07	4.3E-03	11.6	↑
24 h treatment					
MAP2	Microtubule-associated protein 2	5.7E-05	2.3E-02	-15.4	↓
CLIC3	Chloride intracellular channel 3	5.3E-06	2.3E-02	-12.5	↓
PRUNE2	Prune homolog 2 (Drosophila)	5.9E-04	2.3E-02	-10.7	↓
KCNU1	Potassium channel, subfamily U, member 1	1.2E-05	2.3E-02	-10.1	↓
TNNC1	Troponin C type 1 (slow)	3.9E-04	2.3E-02	-9.8	↓
SPOCK3	Sparc/osteonectin, cwcv and kazal-like domains proteoglycan (testican) 3	5.4E-05	2.3E-02	-8.4	↓
PRSS56	Protease, serine, 56	1.5E-04	2.3E-02	-8.1	↓
C1orf140	Uncharacterized LOC400804	3.3E-04	2.3E-02	-8.0	↓
TP53INP1	Tumor protein p53 inducible nuclear protein 1	5.7E-05	2.3E-02	-7.5	↓
LGSN	Lengsin, lens protein with glutamine synthetase domain	9.2E-05	2.3E-02	-7.4	↓
LTBP1	Latent transforming growth factor beta binding protein 1	4.5E-04	2.3E-02	-7.4	↓
FLJ37201	Tigger transposable element derived 2	1.9E-05	2.3E-02	-6.6	↓
ITGBL1	Integrin, beta-like 1 (with EGF-like repeat domains)	6.8E-06	2.3E-02	-6.6	↓
ITGA1	Integrin, alpha 1	6.1E-04	2.3E-02	-6.5	↓
ASZ1	Ankyrin repeat, SAM and basic leucine zipper domain containing 1	7.8E-05	2.3E-02	-6.3	↓
SEMA3D	Sema domain, immunoglobulin domain (Ig), short basic domain, secreted, (semaphorin) 3D	1.7E-04	2.3E-02	-6.0	↓
OLFML2A	Olfactomedin-like 2A	1.7E-04	2.3E-02	-6.0	↓
COL12A1	Collagen, type XII, alpha 1	3.7E-04	2.3E-02	-6.0	↓
INSL4	Insulin-like 4 (placenta)	4.7E-05	2.3E-02	-5.9	↓

Supervised hierarchical clustering (**Figure 7**) over most variable significantly differentially expressed genes in **RuT$_7$** treated cells at 12 and 24 h is depicting time-dependent changes in **RuT$_7$** activity on cellular gene expression profile reflected by the reduction in the number of downregulated genes at 24 h.

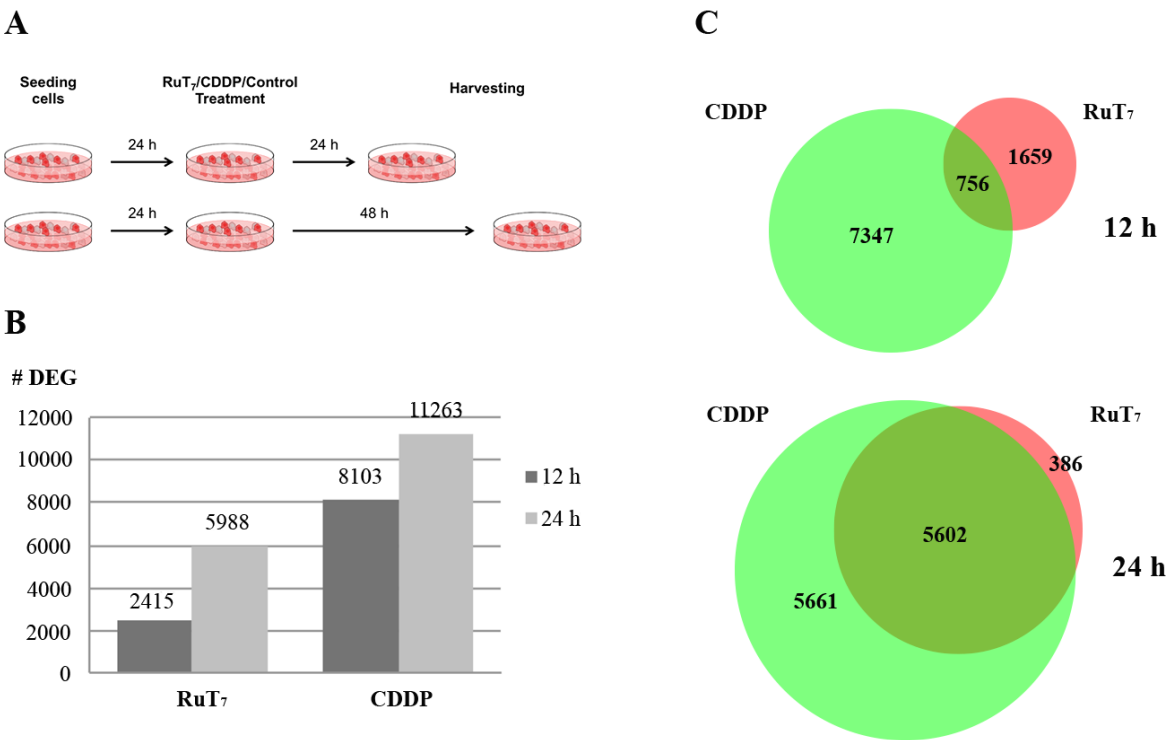

Figure 6. **A.** Experimental procedure outline **B.** Number of differentially expressed genes (DEG) at 12 and 24 h in HeLa cells treated with **RuT7** or CDDP compared to control. **C.** Venn diagrams representing specific and commonly deregulated genes (FDR<0.05 and FC>2) in HeLa cells at 12 and 24 h upon treatment with **RuT7** (in red) and CDDP (in green)

Conversely, cisplatin treatment induced strikingly greater level of gene expression perturbations at both 12 and 24 h, with a total of 8103 (96 upregulated and 8025 downregulated) and 11263 differentially expressed genes (998 upregulated and 10416 downregulated), respectively. At 12 h, cisplatin induced extensive gene expression perturbation with 7347 CDDP-specific DEG, in contrast to moderate changes in gene expression in **RuT7** treated cells (1659 **RuT7**-specific DEG), with only 756 genes commonly deregulated genes between **RuT7** and CDDP treated cells (**Figure 6C**). After 24 h treatment, more prominent changes in gene expression were observed in **RuT7** treated cells, with ~60% of **RuT7**-dependent genes being also deregulated in cisplatin treated cells.

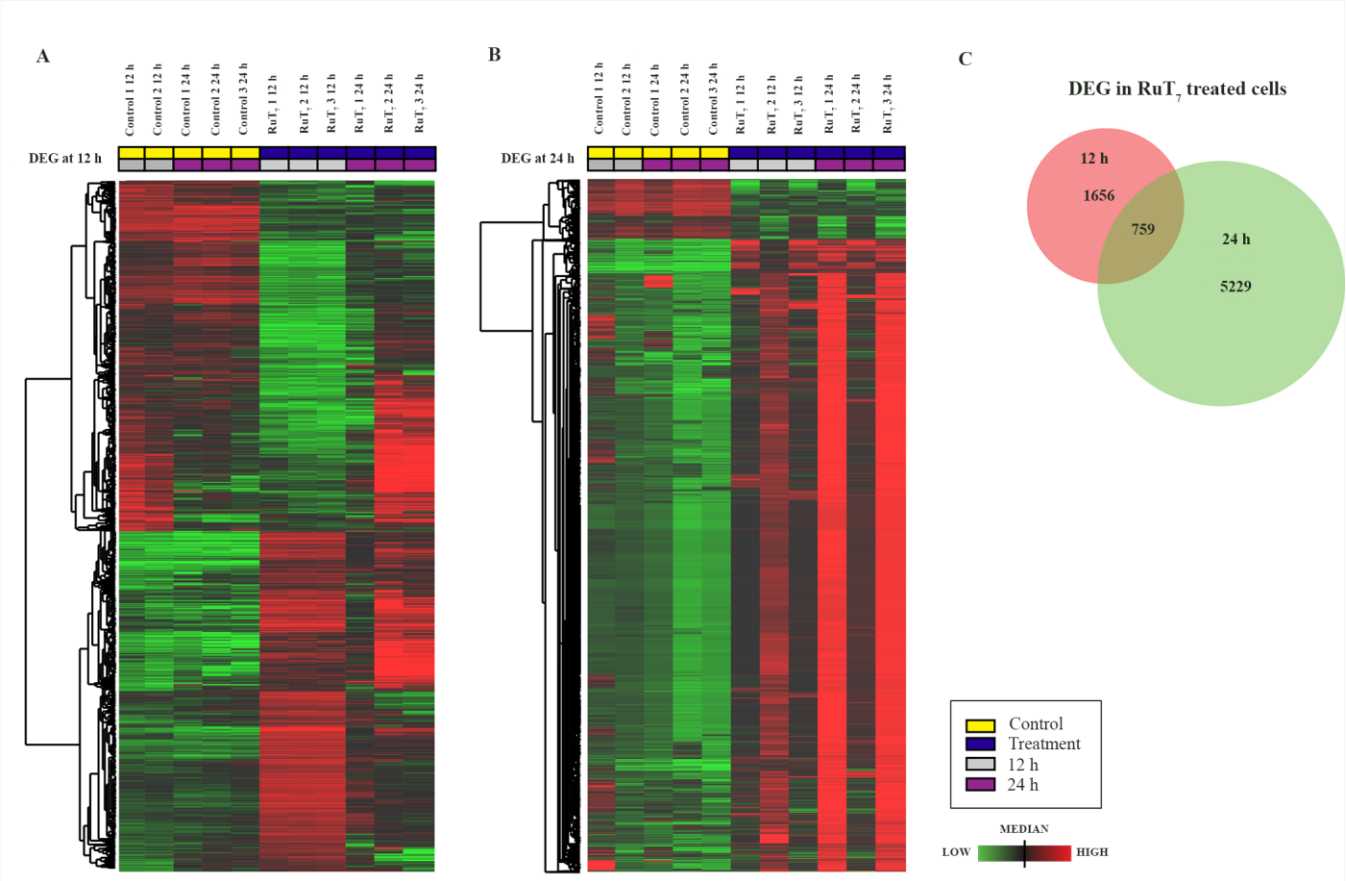

Figure 7. Heatmap representing supervised hierarchical clustering over most variable (above mean standard deviation) significantly differentially expressed genes between **RuT$_7$** and control treated HeLa cells. **A)** at 12 h; **B)** at 24 h. Genes expressed above median are pseudo-colored in red, bellow median in green. **C)** Venn diagram showing specific and common differentially expressed genes in HeLa cells treated with **RuT$_7$** at 12 and 24 h.

3.6 Kinetics and functional analysis of RuT$_7$-induced gene expression changes

Through differential expression analysis we observed time-dependent changes in expression in **RuT$_7$** treated HeLa cells. Gene expression profiles of **RuT$_7$** treated HeLa cells are markedly different after 12 h (**Figure 7A**) and 24 h (**Figure 7B**), with only 759 commonly deregulated genes at both time points (**Figure 7C**).

To identify drug-specific genes and to further explore the kinetics of gene expression changes in cells treated with **RuT$_7$** complex we applied a multivariate regression-based algorithm MaSigPro. The analysis highlighted 5790 genes clustered in 9 co-expressed sets of genes whose expression patterns

show significant changes between 12 and 24 h time points, that differ between **RuT$_7$** treated cells and control population (**Figure 8**). Full list of genes belonging to each cluster and associated coefficients and p-values are represented in **Supplementary Table 5**. To determine the biological relevance of gene expression changes associated with each cluster independently, we an over-representation analysis using Gene Ontology Enrichment Analysis Software Toolkit (GOEAST) that allows determination of significantly enriched GO terms within a gene set, compared with the frequency among all genes on the array. This analysis aimed at an understanding of the effect of the modulation of gene expression on a particular functional categories (biological process, molecular function, and cellular component). Full list of GO categories identified as significantly enriched ($p < 0.01$) among the genes is shown in **Supplementary Tables 6-14**.

Drug-induced changes in gene expression were observed for Cluster 2, Cluster 3 and Cluster 5 genes. Cluster 2 with 2938 highly expressed genes that were consistently downregulated, while 540 genes belonging to Cluster 3 were consistently upregulated in **RuT$_7$** treated cells with similar degree of time-dependent changes in control and **RuT$_7$** treated cells. Genes belonging to Cluster 5 (1470) were induced in **RuT$_7$** treated cells while being expressed at a constant rate over time in control cells. Functional characterization of genes belonging to drug-specific genes clusters with constant response (Cluster 2, 3 and 5) indicated that Cluster 2 was significantly enriched for GO molecular functions related specifically to hydrolase and oxidoreductase catalytic activity and ion binding, while significantly enriched biological functions inculded organic substance metabolic process and ATPase activity coupled to transmembrane movement of ions. Both Cluster 3 and Cluster 5 genes were significantly enriched for molecular functions related to nucleic acid binding, heterocyclic compound bounding and transition metal ion binding, where top biological functions were related to general metabolic processes.

Early response genes following **RuT$_7$** treatment were identified in Cluster 6 (930) showing strong induction at 12 h followed by a drop in expression at 24 h to the level of control cells, and in Cluster 8 with 649 genes that were repressed at 12 h in **RuT$_7$** treated cells followed by an increase in expression at 24 h. Significantly enriched molecular functions for upregulated early response genes belonging to

Cluster 6 included nucleic acid binding, heterocyclic compound bounding and transition metal ion binding in addition to histone methyltransferase activity and biological processes histone acetylation, negative regulation of transcription and intrinsic apoptotic signaling pathway in response to DNA damage by p53 class mediator. Downregulated early response genes (Cluster 8) had only a few significant molecular function among which are WW domain binding and transferase activity, transferring acyl groups molecular function and regulation of spindle organization and M phase of mitotic cell cycle as biological processes localized to cellular compartments Ndc80 complex, nuclear chromosome and centrosome.

RuT$_7$ treatment-specific genes with delayed response were identified in Cluster 1 and Cluster 7. Cluster 1 contained 2722 low-expressed genes which demonstrated significant change in induction along time, while 410 highly expressed genes in Cluster 7 were significantly repressed at 24 h. G-protein coupled receptor activity, intracellular cAMP activated cation channel activity, ignal transducer activity and cell communication and esponse to stimulus were significantly over-represented among upregulated low expressed late response genes belonging to Cluster 1 with cellular compartment localization to plasma membrane, and intermediate filaments. Top GO terms for downregulated late response genes belonging to Cluster 7 included enzyme regulator activity, protein serine/threonine kinase inhibitor activity and mismatch base pair DNA N- glycosilase activity, nuclear replication fork, microtubule organizing centre, regulation of cyclin-dependant serine/threonine kinase activity and regulation of transcription involved in G1/S phase of mitotic cell cycle.

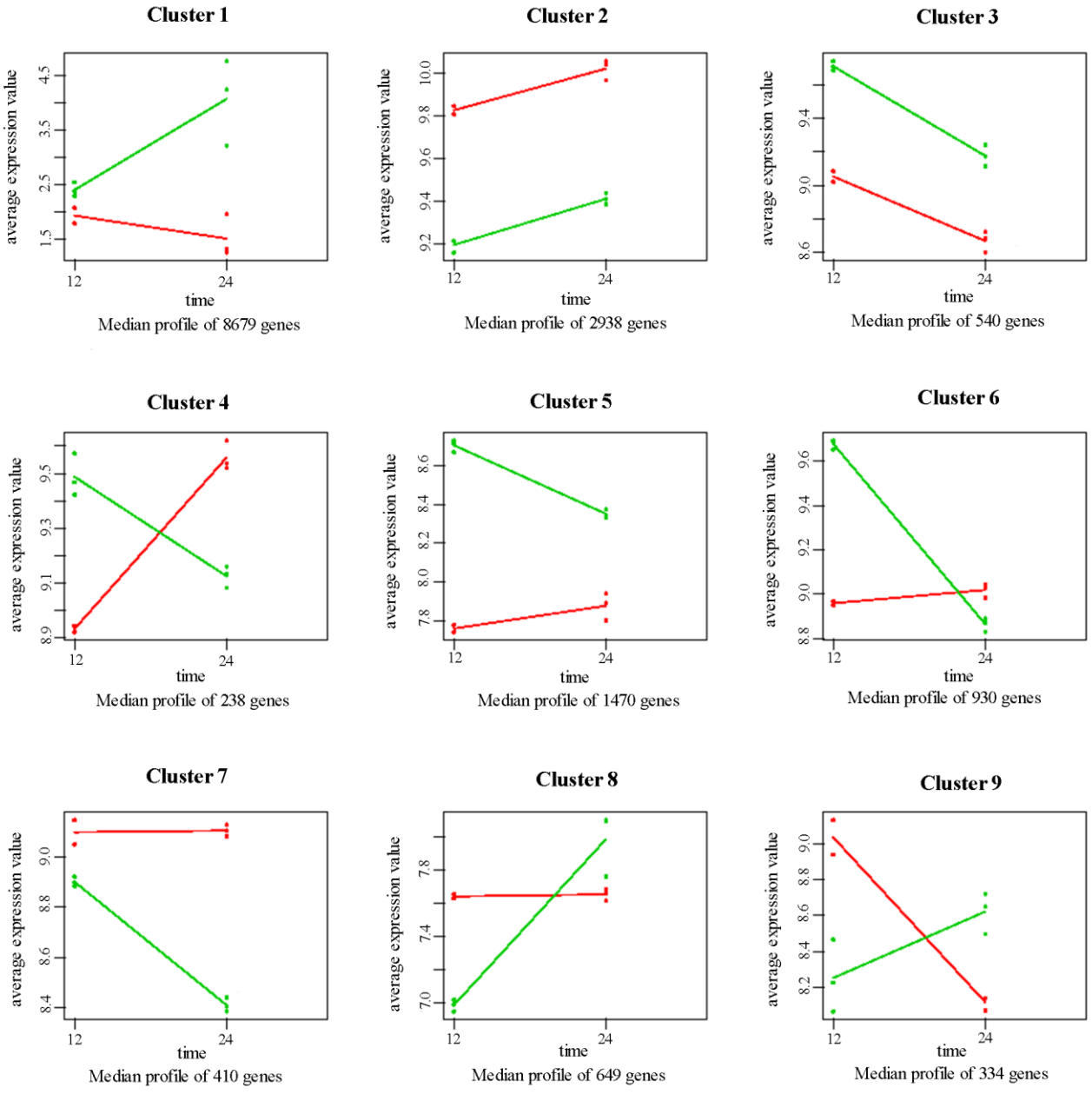

Figure 8. Group plots show the direction of expression changes for each gene cluster over time (12 h and 24 h) measurements and the differences between the **RuT**$_7$ (green) and control-treated cells (red). Genes are clustered by similar patterns and an average gene expression level is represented for each cluster, with associated 95% CI (upper and lower dots). The slope coefficient represents the values of the estimated regression coefficients, positive for induced gene clusters, negative for repressed gene clusters.

RuT$_7$ treatment showed strong effect modification on expression of time-dependent genes belonging to Cluster 4 (238 genes) and Cluster 9 (334 genes). Cluster 4 genes (238) were induced by

RuT$_7$ treatment at 12 h followed by a significant drop in expression at 24 h, in contrast to control treated cells exhibiting inverse direction of changes of expression, while genes belonging to Cluster 9 had opposite direction of expression changes.

3.7 Differences in toxicity profiles of RuT$_7$ and CDDP treated HeLa cells

Cell cycle analysis highlighted differences in cellular response to RuT7 and CDDP. To gain better understanding of the underlying biological processes in **RuT$_7$** or CDDP treated cells at 12 and 24 h time points, we interrogated the list of the differentially expressed genes using Ingenuity Pathway Analysis® software (IPA, Ingenuity Systems, Redwood City, CA). All canonical pathways, biological functions and networks significantly enriched in **RuT$_7$** and CDDP treated cells at 12 and 24 h time points are represented in **Supplementary Tables 15-18**.

Both at 12 and 24 h top enriched biological functions in **RuT$_7$** treated cells were related to ell death and survival, cellular compromise, nucleic acid metabolism, small molecule biochemistry, cell-to-cell signaling and interaction, molecular transport, cellular development, cellular growth and proliferation, drug metabolism and cell cycle. Additionally, at 12 h HeLa cells treated with **RuT$_7$** show significant enrichment of genes belonging to RNA damage and repair, free radical scavenging, DNA replication, recombination and repair, protein synthesis, protein trafficking biological functions. Canonical pathways enriched both at 12 and 24 h in **RuT$_7$** treated cells included estrogen biosynthesis, agranulocyte adhesion and diapedesis, and metabolic degradation pathways.

We examined genes and pathways differentially modulated in response to **RuT$_7$** and CDDP. While many pathways and biological functions were commonly enriched (**Supplementary Figures 1-2**), there were specific effects of **RuT$_7$** reflected by the induction of genes belonging to estrogen biosynthesis and metabolite degradation canonical pathways, while CDDP treated cells had markedly stronger association with calcium transport and citruline metabolism canonical pathways and biological functions of antimicrobial response and molecular transport. To predict potential toxicities associated with **RuT$_7$** treatment we performed IPA Tox Comparison Analysis on differentially expressed genes at 12 and 24 h and compared it to CDDP toxicity profile. There were significant differences in the

predicted toxicity profile (**Figure 9**), with CDDP-treated cells showing strong enrichment at 24 h for genes involved in cardiac arrhythmia, cardiac infarction and kidney failure whle **RuT7** had no significantly associated toxicity functions.

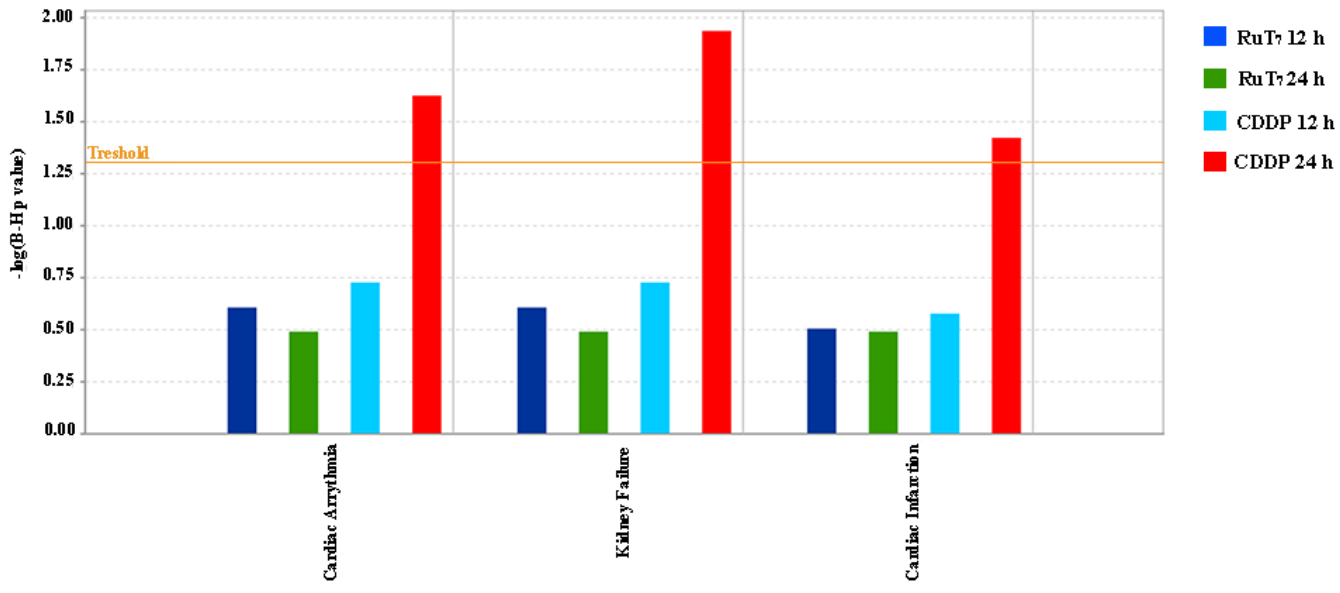

Figure 9. Bar chart depicting significantly enriched (FDR<0.05) toxicity functions determined by IPA Tox Comparison Analysis

4. Discussion

Extensive investigations of alternative transition metal-based cancer therapies to platinum-based drugs have been conducted since the initial discovery of cisplatin anticancer properties [34]. Ruthenium-based compounds have emerged as promising drug candidates because of their properties such as the rate of ligand exchange, the range of accessible oxidation states and the ability of ruthenium to mimic iron in binding to certain biological molecules [35]. Lately, ruthenium(II)-arene complexes are in the limelight of ruthenium-based anticancer compound research, due to their stability, water solubility and structure manipulation susceptibility, providing space for design optimization, which works in terms of increasing their biological activity and minimizing side-effects [36]. In our present study, besides investigation of *in vitro* cellular response, for the first time, whole-transcriptome microarray gene expression analysis in HeLa cells treated with ruthenium(II)-arene complex has been

performed in order to elucidate gene expression alterations in cancer cells after ruthenium-based drug exposure. Predicted toxicity profiles for **RuT$_7$** and CDDP have also been assessed and compared.

Inhibition of DNA replication is well-known feature of cisplatin mechanism of action, which is reflected in our data through accumulation of cells in S phase after CDDP treatment [37]. Likewise, arrest in the S phase of cell cycle indicates possible binding to and/or damage of DNA by **RuT$_7$** complex, leading to consequent replication inhibition of cancer cells. With lower concentrations of **RuT$_7$** applied (0.5 x IC_{50}), prominent S phase accumulation is obtained. These results are in the compliance with our previous study of the biological activity of similar ruthenium complexes [Ru(η^6-*p*-cymene)(L)Cl_2], where complex with picolinic acid as ligand (L) exerted it´s cytotoxic effect through S phase cell cycle arrest and significant intracellular distribution in DNA, rather than protein fraction of treated cells, indicating DNA as target of its action [38]. After 24 h of continual treatment of HeLa cells with **RuT$_7$**, an observed increase of Sub-G1 phase denotes apoptotic and/or necrotic population of cells. However, doubling the concentration of **RuT$_7$** increases sub-G1 population of HeLa cells drastically, that may be interpreted as contribution of general toxicity of **RuT$_7$** complex. This hypothesis is also supported by the apparent decrease in the S and G1 phase subpopulations compared to control, and points out the importance of determining the proper concentration of drug.

After 48 h of incubation, RuT_7 progressively induced S arrest in a concentration-dependent manner, which was accompanied by a parallel decrease in the G1 population. . It should be pointed out that after **RuT$_7$** treatment, significantly higher number of cells proceeds to G2 phase, compared to CDDP, which possibly indicate different mechanism of action of **RuT$_7$** complex and CDDP.

Phosphatidylserine (PS) externalization is one of early hallmarks that denote apoptosis, the process of programmed cell death. Annexin V, a Ca^{2+}-dependent phospholipid-binding protein, has high affinity for PS, and in conjunction with the proper fluorochrome, fluorescein isothiocyanate (FITC) can be used for detection of exposed apoptotic cell surface PS [39, 40]. After treatment with **RuT$_7$** that lasted 24 h, HeLa cells exposing PS on its surface were monitored. Compared to control, an increase in early apoptotic cell fraction (FITC(+)/PI(-)) was not obtained, neither for **RuT$_7$** complex nor CDDP. However, there is a prominent increase in late apoptotic and/or already dead cells (FITC(+)/PI(+)), as

well as increase in dead cells number (FITC(-)/PI(+)) after **RuT$_7$** treatment (**Figure 3**). Absence of early apoptotic fraction of cells can be explained by possible fast and immediate action of **RuT$_7$** complex, where after 24 h of incubation period majority of early apoptotic cells have already proceeded to late apoptotic stage. These results are in correlation with the appearance of sub-G1 fraction of cells in cell cycle phase distribution analyses (**Figure 2**).

Typical morphological features of the apoptotic cells are highly condensed nuclei, cell shrinkage and formation of apoptotic bodies. In the early apoptosis, only acridine orange enters the cell with ethidium bromide excluded and the nucleus stains green. In the late apoptosis along with the loss of membrane integrity, both dyes enter the cell and the nucleus becomes orange-red [41]. After only 3 h of treatment with **RuT$_7$**, changes in morphological features of HeLa cells are obvious, when compared to control HeLa cells. Decreased density/cell number, round shape and beginning of nuclear condensation are the most prominent features after 3 h of treatment. Already after 5 h of incubation with **RuT$_7$**, highly condensed nuclei and membrane blebbing are predominant hallmarks. These findings, together with photomicrographs obtained after 24 h of continual treatment are in concordance with the results of Annexin V-FITC assay, and represent confirmation of hypothesized fast, nearly immediate **RuT$_7$** action. The continuous presence of cells with apoptotic morphology can be explained with persistent intracellular accumulation of **RuT$_7$** (**Figure 5**). Morphological analysis by fluorescence microscopy of acridine orange/ethidium bromide-stained HeLa cells exposed to **RuT$_7$** has undoubtedly proven apoptosis-inducing potential of investigated complex, which is one of the main prerogatives for successful chemotherapeutic agent.

ICP-MS analysis of total intracellular accumulation of ruthenium has shown time-dependent increase of intracellular ruthenium content. High intracellular ruthenium concentration already after 6 h of incubation (8.83 ± 0.09 ng Ru/10^6 cells) is in agreement with previous conclusions about very fast action of **RuT$_7$**. Our assumption is that **RuT$_7$** enters cell very fast, which implicates possible passive transmembrane transport of this compound. Due to the presence of arene ligand [42-44], as well as isoquinoline-3-carboxylic acid (derivative of picolinic acid with fused phenyl group), which significantly contribute to lipophilicity of the complex [45-52], passive transport through hydrophobic

lipid bilayer is plausible. Through the course of time, ruthenium holds and even increases its concentration inside cells (24 and 48 h incubation, respectively, **Figure 5**). This implicates binding of **RuT$_7$** to intracellular structures and its continuous accumulation in intracellular environment [53].

It is clear from the results above that, on cellular level, **RuT$_7$** exhibited cytotoxic effect comparable to CDDP. However, this effect is reflected on molecular level as more subtle perturbation of HeLa cell transcriptome. Besides overall lower level of gene expression perturbations induced by **RuT$_7$** complex, different mechanism of action is visible from schematic representation of specific and commonly deregulated genes in HeLa cells at 12 h and 24 h upon treatment with **RuT$_7$** and CDDP (Venn diagrams, **Figure 6C**). After 12 h of treatment, 1659 **RuT$_7$**-specific DEG has been found, which were not deregulated in CDDP-treated population. These results provide evidence that, during this 'early response' to treatment (12 h), different molecular mechanisms are active after **RuT$_7$** and CDDP treatment.

Analysis of gene clusters with similar expression patterns gave us valuable informations concerning mechanism of **RuT$_7$** actionRuT7-treatment induced consistent upregulation –of genes implicated in nucleic acid binding, heterocyclic compound bounding and transition metal ion binding (Clusters 3, 5 and 6). Besides the strong implication of DNA binding of **RuT$_7$** inside the living cell, these data also provide information about interactions of transition metal by itself, as well as interaction of heterocyclic ligand with cells' genetic material. This could possibly indicate binding of the whole organometallic complex to cells' DNA, as previously demonstrated *in vitro* [12], which confirms its stability in physiological conditions. Moreover, upregulation of early response genes of Cluster 6 that are included in GO biological functions Histone histone acetylation, negative regulation of transcription and intrinsic apoptotic signaling pathway in response to DNA damage by p53 class mediator, clearly indicate activation of the DNA damage response (DDR), which represents a coordinated series of events that regulates cell cycle progression and repair of DNA lesions, as well as increasing the accessibility of the repair machinery to lesions embedded in chromatin [54]. Enrichment of intrinsic apoptotic signaling pathway in response to DNA damage by p53 class mediator, provides a strong confirmation of results obtained by flow cytometry and acridine orange/ethidium bromide staining. As

hypothesized, apoptotic signaling pathway takes place shortly after **RuT$_7$** treatment (Cluster 6 genes showing strong induction at 12 h), consequently yielding large number of late apoptotic and/or dead cells at 24 h time point (**Figure 3**).

Downregulated early response genes included in Cluster 8, describing biological functions of Regulation of spindle organization and M phase of mitotic cell cycle, indicate possible mitosis inhibition. There are numerous literature data about ruthenium(III) complexes exhibiting similar mechanism of action [55-58]. Likewise, significantly repressed late response genes (at 24 h) belonging to Cluster 7, included in Regulation of transcription involved in G1/S phase of mitotic cell cycle and similar biological functions, denotes treatment-induced G1/S phase arrest. This is in a good agreement with our results of cell cycle analysis, where 0.5 x IC_{50} concentration-induced S-phase arrest after 24 h of treatment is prominent feature (**Figure 2**).

In further analysis we tried to shed light on involvement of DEGs in specific biological functions and canonical pathways, and to further elucidate possible mechanisms of action of **RuT$_7$** complex. After 12 h of **RuT$_7$** treatment, Free radical scavenging enrichment could point out on oxidative stress of HeLa cells, which can result from presence of reactive oxygen species. This enriched biological function could be connected to DNA Replication, Recombination and Repair and RNA Damage and Repair enriched functions, which indicate damage in DNA/RNA molecules, possibly caused by the generation of free radicals inside the cell. This is consistent with the literature data about ruthenium based complexes mechanism of action [18]. Besides DNA/RNA damage due to direct binding of **RuT$_7$** complex to these molecules already discussed before, these findings could point out to alternative mechanism of **RuT$_7$** action. Protein synthesis and Protein trafficking are biological functions also exclusively enriched after 12 h of incubation of HeLa cells with the investigated compound. These functions could be connected to aforementioned DNA damage, because cell needs complex protein machinery for DNA repair and/or replication processes, as well as for cell cycle arrest and driving cell to apoptosis [37, 59-62]. This is also in agreement with top GO enriched biological functions in Clusters 7 and 8, describing G1/S and G2/M arrest, respectively.

Cellular growth and Proliferation, Cell cycle and Cell death are biological functions enriched at 12 and 24 h that could be as well considered as confirmation of aforementioned results. Together, these functions describe genes associated with the growth and proliferation of cells, as well as stages of the cell cycle including cell division. Overall, these results, together with flow cytometry experiments, strongly indicate role of **RuT$_7$** in the cell cycle progression inhibition. Other commonly enriched biological functions for both incubation times (12 h and 24 h) worth mentioning are Cell-To-Cell signaling and Interaction together with Cellular compromise. These clearly indicate that after 12 h of treatment (and 24 h also) effects of **RuT$_7$** complex include disruption and damage of cells that are preceded by compromising intercellular junctions and/or cell-surface contacts. Our results of morphological analysis of HeLa cells treated with **RuT$_7$** complex and stained with AO/EtBr have shown that already after 3 h of treatment, cells begin to lose their normal morphology, contacts with other cells and become detached from the surface (**Figure 5**). This compromising of cells' function through the direct damage of plasma membrane could be considered as a repercussion of redox activity of **RuT$_7$**. It seems that, besides inducing oxidative stress inside the cell, ruthenium(II)-arene complex works directly on plasma membrane through still obscure mechanisms of action.

Although functional gene profiling analysis revealed 12 h treatment-specific biological functions, after 24 h of incubation of HeLa with **RuT$_7$** complex there were no biological functions that were specific for this incubation period. On the contrary, number of enriched functions decreases after 24 h, but number of genes involved in the remaining (commonly enriched) functions increases. This, once again, puts emphasis on action dynamics of **RuT$_7$** complex.

One of the major aspects of introducing new chemotherapeutics in clinical practice is certainly the assessment of its potential systemic toxicity. IPA Tox Comparison Analysis on differentially expressed genes at 12 and 24 h revealed significant differences in the predicted toxicity profile between **RuT$_7$** and CDDP (**Figure 9**). For genes involved in cardiac arrhythmia, cardiac infarction and kidney failure, CDDP-treated cells show strong enrichment of genes involved in these diseases for 24 h treatment, while same toxicity functions are far below threshold for **RuT$_7$**-treated cells. These results that elucidate molecular basis of CDDP toxicity are in concordance with the existing data on patients [63-66]. These

findings clearly demonstrate that ruthenium(II)-arene complex does not exhibit the same toxicity pattern as CDDP. According to analyzed microarray data, conclusion that **RuT$_7$** complex leads HeLa cells through the intrinsic (mitochondrial) apoptotic pathway can be made. It seems that DNA damage is made by the action of reactive oxygen species and through the direct DNA binding of organometallic complex. This first triggers various biological processes connected to M phase of mitotic cell cycle (downregulated early response genes within Cluster 8), followed by chromatin remodeling and DNA repair events (upregulated early response genes belonging to Cluster 6), leading eventually to blockage of DNA synthesis (downregulated late response genes belonging to Cluster 7). Literature data about mechanism of action of various ruthenium-based complexes supporting our experimental results are numerous [2, 56, 67-71]. Having in mind different mechanism of action of ruthenium(II)-arene complexes compared to CDDP, as well as differences in the predicted toxicity profiles, further efforts should be oriented towards the inclusion of these compounds in animal and pre-clinical studies as potential drug candidates.

Abbreviations

AO acridine orange

CDDP *cis*-diamminedichloroplatinum(II)

CT calf thymus

DEG differentially expressed gene

DMSO dimethyl sulfoxide

DMF dimethylformamide

EB ethidium bromide

FCS fetal calf serum

GOEAST Gene Ontology Enrichment Analysis Software Toolkit

HeLa Henrietta Lacks

HEPES 4-(2-Hydroxyethyl)piperazine-1-ethanesulfonic acid

ICP-MS Inductively coupled plasma mass spectrometry

IPA Ingenuity Pathway Analysis

lncRNA Long non-coding RNA

MTT 3-(4,5-dimethylthiazol-2-yl)-2,5-diphenyltetrazolium bromide

PBS phosphate-buffered saline

PI propidium iodide

Roswell Park Memorial Institute RPMI

Acknowledgements

This work was supported by the Ministry of Education, Science and Technological Development of Serbia (Grant No. III 41026, OI 172017 and OI 172030).

Conflict of interest

The authors declare no competing financial interest.

References

[1] I. Kostova, Curr. Med. Chem. 13 (2006) 1085-1107.

[2] C. Gaiddon, P. Jeannequin, P. Bischoff, M. Pfeffer, C. Sirlin, J.P. Loeffler, J. Pharmacol. Exp. Ther. 315 (2005) 1403-1411.

[3] A. Bergamo, C. Gaiddon, J.H. Schellens, J.H. Beijnen, G. Sava, J. Inorg. Biochem. 106 (2012) 90-99.

[4] W.H. Ang, P.J. Dyson, Eur. J. Med. Chem. 20 (2006) 4003-4018.

[5] P.C. Bruijnincx, P.J. Sadler, Curr. Opin. Chem. Biol. 12 (2008) 197-206.

[6] E. Reisner, V.B. Arion, B.K. Keppler, A.J. Pombeiro, Inorg. Chim. Acta. 361 (2008) 1569-1583.

[7] G. Sava, A. Bergamo, P.J. Dyson, Dalton Trans. 40 (2011) 9069-9075.

[8] S. Kapitza, M. Pongratz, M. Jakupec, P. Heffeter, W. Berger, L. Lackinger, B.K. Keppler, B. Marian, J. Cancer Res. Clin. Oncol. 131 (2005) 101-110.

[9] P.S. Kuhn, G.E. Buchel, K.K. Jovanovic, L. Filipovic, S. Radulovic, P. Rapta, V.B. Arion, Inorg. Chem. 53 (2014) 11130-11139.

[10] P.J. Dyson, CHIMIA Int. J. Chem. 61 (2007) 698-703.

[11] G. Süss-Fink, Dalton Trans. 39 (2009) 1673-1688.

[12] I. Ivanović, K.K. Jovanović, N. Gligorijević, S. Radulović, V.B. Arion, K.S.A. Sheweshein, Ž.L. Tešić, S. Grgurić-Šipka, J. Organomet. Chem. 749 (2014) 343-349.

[13] S. Shi, J. Liu, J. Li, K.C. Zheng, X.M. Huang, C.P. Tan, L.M. Chen, L.N. Ji, J. Inorg. Biochem. 100 (2006) 385-395.

[14] G. Sava, S. Zorzet, C. Turrin, F. Vita, M. Soranzo, G. Zabucchi, M. Cocchietto, A. Bergamo, S. DiGiovine, G. Pezzoni, L. Sartor, S. Garbisa, Clin. Cancer Res. 9 (2003) 1898-1905.

[15] A. Bergamo, A. Masi, P.J. Dyson, G. Sava, Int. J. Oncol. 33 (2008) 1281-1289.

[16] V. Moreno, M. Font-Bardia, T. Calvet, J. Lorenzo, F.X. Aviles, M.H. Garcia, T.S. Morais, A. Valente, M.P. Robalo, J. Inorg. Biochem. 105 (2011) 241-249.

[17] A. Martinez, J. Suarez, T. Shand, R.S. Magliozzo, R.A. Sanchez-Delgado, J. Inorg. Biochem. 105 (2011) 39-45.

[18] S. Kapitza, M.A. Jakupec, M. Uhl, B.K. Keppler, B. Marian, Cancer Lett. 226 (2005) 115-121.

[19] K.J. Du, J.Q. Wang, J.F. Kou, G.Y. Li, L.L. Wang, H. Chao, L.N. Ji, Eur. J. Med. Chem. 46 (2011) 1056-1065.

[20] R. Gaur, L. Mishra, Inorg. Chem. 51 (2012) 3059-3070.

[21] L. Li, Y.S. Wong, T. Chen, C. Fan, W. Zheng, Dalton Trans. 41 (2012) 1138-1141.

[22] A.A. Nazarov, M. Baquié, P. Nowak-Sliwinska, O. Zava, J.R.v. Beijnum, M. Groessl, D.M. Chisholm, Z. Ahmadi, J. McIndoe, A. Griffioen, H.v.d. Bergh, Sci. Rep. 3 (2013) 1485.

[23] P. Nowak-Sliwinska, J.R. van Beijnum, A. Casini, A.A. Nazarov, G. Wagnieres, H. van den Bergh, P.J. Dyson, A.W. Griffioen, J. Med. Chem. 54 (2011) 3895-3902.

[24] A. Bergamo, M. Gerdol, M. Lucafo, C. Pelillo, M. Battaglia, A. Pallavicini, G. Sava, Metallomics. 7 (2015) 1439-1450.

[25] A. Grozav, O. Balacescu, L. Balacescu, T. Cheminel, I. Berindan-Neagoe, B. Therrien, J. Med. Chem. 58 (2015) 8475-8490.

[26] M.G. Ormerod (Ed.), Analysis od DNA - general methods. In Flow Cytometry: A Practical Approach, Oxford University Press, Oxford, 2000.

[27] P. Heitland, H.D. Koster, Clin. Chim. Acta. 365 (2006) 310-318.

[28] Y. Benjamini, D. Drai, G. Elmer, N. Kafkafi, I. Golani, Behav. Brain. Res. 125 (2001) 279-284.

[29] M.B. Eisen, P.T. Spellman, P.O. Brown, D. Botstein, Proc. Natl. Acad. Sci. U S A. 95 (1998) 14863-14868.

[30] M.J. Nueda, S. Tarazona, A. Conesa, Bioinformatics. 30 (2014) 2598-2602.

[31] A. Conesa, M.J. Nueda, A. Ferrer, M. Talon, Bioinformatics. 22 (2006) 1096-1102.

[32] Q. Zheng, X.J. Wang, Nucleic Acids Res. 36 (2008) W358-363.

[33] Y. Benjamini, D. Yekutieli, Ann. Stat. 29 (2001) 1165-1188.

[34] Y.P. Ho, S.C. Au-Yeung, K.K. To, Med. Res. Rev. 23 (2003) 633-655.

[35] C.S. Allardyce, P.J. Dyson, Platinum Met. Rev. 45 (2001) 62-69.

[36] Y.K. Yan, M. Melchart, A. Habtemariam, P.J. Sadler, Chem. Commun (Camb). (2005) 4764-4776.

[37] G. Chu, J. Biol. Chem. 269 (1994) 787-790.

[38] N. Gligorijevic, S. Arandelovic, L. Filipovic, K. Jakovljevic, R. Jankovic, S. Grguric-Sipka, I. Ivanovic, S. Radulovic, Z. Tesic, J. Inorg. Biochem. 108 (2012) 53-61.

[39] I. Vermes, C. Haanen, H. Steffens-Nakken, C. Reutelingsperger, J. Immunol. Methods. 184 (1995) 39-51.

[40] L. Casciola-Rosen, A. Rosen, M. Petri, M. Schlissel, Proc. Natl. Acad. Sci. U S A. 93 (1996) 1624-1629.

[41] S. Kasibhatla, G.P. Amarante-Mendes, D. Finucane, T. Brunner, E. Bossy-Wetzel, D.R. Green, CSH Protoc. 2006 (2006)

[42] F. Giannini, L. Geiser, L.E. Paul, T. Roder, B. Therrien, G. Süss-Fink, J. Furrer, J. Organomet. Chem. 783 (2015) 40-45.

[43] W. Su, Z. Tang, Q. Xiao, P. Li, Q. Qian, X. Lei, S. Huang, B. Peng, J. Cui, C. Huang, J. Organomet. Chem. 783 (2015) 10-16.

[44] R.E. Morris, R.E. Aird, S. Murdoch Pdel, H. Chen, J. Cummings, N.D. Hughes, S. Parsons, A. Parkin, G. Boyd, D.I. Jodrell, P.J. Sadler, J. Med. Chem. 44 (2001) 3616-3621.

[45] R. Song, K.M. Kim, Y.S. Sohn, Inorg. Chim. Acta. 292 (1999) 238-243.

[46] D.M. Stearns, W.H. Armstrong, Inorg. Chem. 31 (1992) 5178-5184.

[47] N.E. Chakov, R.A. Collins, J.B. Vincent, Polyhedron. 18 (1999) 2891-2897.

[48] H. Ding, L.K. Olson, J.A. Caruso, Spectrochim. Acta. 51 (1996) 1801-1812.

[49] D.D. Hepburn, J. Xiao, S. Bindom, J.B. Vincent, J. O'Donnell, Proc. Natl. Acad. Sci. U S A. 100 (2003) 3766-3771.

[50] D.M. Stearns, S.M. Silveira, K.K. Wolf, A.M. Luke, Mutat. Res. 513 (2002) 135-142.

[51] G.S. Morris, K.A. Guidry, M. Hegsted, D.L. Hasten, Nutr. Res. 15 (1995) 1045-1052.

[52] Y. Liang, L.K. Noda, O. Sala, J. Mol. Struct. 554 (2000) 271-277.

[53] P.S. Kuhn, L. Cremer, A. Gavriluta, K.K. Jovanovic, L. Filipovic, A.A. Hummer, G.E. Buchel, B.P. Dojcinovic, S.M. Meier, A. Rompel, S. Radulovic, J.B. Tommasino, D. Luneau, V.B. Arion, Chemistry. 21 (2015) 13703-13713.

[54] M.S. Luijsterburg, H. van Attikum, Mol. Oncol. 5 (2011) 349-367.

[55] P. Heffeter, B. Atil, K. Kryeziu, D. Groza, G. Koellensperger, W. Korner, U. Jungwirth, T. Mohr, B.K. Keppler, W. Berger, Eur. J. Cancer. 49 (2013) 3366-3375.

[56] A. Bergamo, G. Stocco, B. Gava, M. Cocchietto, E. Alessio, B. Serli, E. Iengo, G. Sava, J. Pharmacol. Exp. Ther. 305 (2003) 725-732.

[57] S. Zorzet, A. Bergamo, M. Cocchietto, A. Sorc, B. Gava, E. Alessio, E. Iengo, G. Sava, J. Pharmacol. Exp. Ther. 295 (2000) 927-933.

[58] A. Bergamo, R. Gagliardi, V. Scarcia, A. Furlani, E. Alessio, G. Mestroni, G. Sava, J. Pharmacol. Exp. Ther. 289 (1999) 559-564.

[59] N.D. Lakin, S.P. Jackson, Oncogene. 18 (1999) 7644-7655.

[60] A. Hirao, Y.Y. Kong, S. Matsuoka, A. Wakeham, J. Ruland, H. Yoshida, D. Liu, S.J. Elledge, T.W. Mak, Science. 287 (2000) 1824-1827.

[61] J. Bartek, J. Lukas, Curr. Opin. Cell Biol. 13 (2001) 738-747.

[62] M. Takagi, M.J. Absalon, K.G. McLure, M.B. Kastan, Cell. 123 (2005) 49-63.

[63] M.T. Meinardi, J.A. Gietema, W.T. van der Graaf, D.J. van Veldhuisen, M.A. Runne, W.J. Sluiter, E.G. de Vries, P.B. Willemse, N.H. Mulder, M.P. van den Berg, H.S. Koops, D.T. Sleijfer, J. Clin. Oncol. 18 (2000) 1725-1732.

[64] R.S. Goldstein, B. Noordewier, J.T. Bond, J.B. Hook, G.H. Mayor, Toxicol. Appl. Pharmacol. 60 (1981) 163-175.

[65] G. Brillet, G. Deray, M. Lucsko, C. Faucher, P. Aubert, J. Rottembourg, C. Jacobs, Nephrologie. 14 (1993) 227-229.

[66] H. Zhou, A. Kato, H. Yasuda, T. Miyaji, Y. Fujigaki, T. Yamamoto, K. Yonemura, A. Hishida, Toxicol. Appl. Pharmacol. 200 (2004) 111-120.

[67] V. Brabec, O. Novakova, Drug Resist. Updat. 9 (2006) 111-122.

[68] G.J. Lin, G.B. Jiang, Y.Y. Xie, H.L. Huang, Z.H. Liang, Y.J. Liu, J. Biol. Inorg. Chem. 18 (2013) 873-882.

[69] S. Chatterjee, S. Kundu, A. Bhattacharyya, C.G. Hartinger, P.J. Dyson, J. Biol. Inorg. Chem. 13 (2008) 1149-1155.

[70] R. Trondl, P. Heffeter, C.R. Kowol, M.A. Jakupec, W. Berger, B.K. Keppler, Chem. Sci. 5 (2014) 2925–2932.

[71] C. Qian, J.Q. Wang, C.L. Song, L.L. Wang, L.N. Ji, H. Chao, Metallomics. 5 (2013) 844-854.

Figure/Table captions

Figure 1. Structure of ruthenium(II)-arene complex **RuT7**, [Ru(η^6-*p*-cymene)(L)Cl]

Figure 2. Effects of **RuT7** and CDDP on cell cycle distribution. Untreated (control) HeLa cells or HeLa cells treated for 24 h (A) and 48 h (B) with 0.5 x IC_{50} and IC_{50} concentrations of **RuT7** (22.7 and 45.4 μM) and CDDP (2.6 and 5.2 μM), respectively. The results are expressed as mean ± standard deviations of three independent experiments.

Figure 3. Apoptosis induction potential of **RuT7** and CDDP. A. Cells were treated for 24 h with 0.5 x IC_{50} and IC_{50} concentrations of **RuT7** (22.7 and 45.4 μM) and CDDP (2.6 and 5.2 μM), respectively; FITC(-)/PI(-) are live cells, FITC(+)/PI(-) are early apoptotic cells, FITC(+)/PI(+) are late apoptotic or necrotic cells and FITC(-)/PI(+) are dead cells. The results are expressed as mean ± standard deviations of three independent experiments

Figure 4. Photomicrographs of acridine orange/ethidium bromide-stained control (C) HeLa cells and HeLa cells exposed for 3 and 5 h to complex **RuT7** (left), and photomicrographs of acridine orange/ethidium bromide-stained control (C) HeLa cells and HeLa cells exposed for 24 h to complex **RuT7** (right). Red arrows point to cytoplasmic shrinkage and nuclear condensation; blue arrows denote membrane blebbing structures. Scale bars in the upper images correspond to magnification of photomicrographs below. Applied concentrations of **RuT7** corresponded to 22.7 μM (0.5 x IC_{50}) values determined for 48 h incubation period

Figure 5. Total intracellular accumulation of ruthenium in HeLa cells after 6, 24 and 48 h, measured by ICP-MS. All experiments were performed in triplicate and presented with corresponding standard deviations (SD).

Table 1. Top-20 significantly differentially genes in **RuT7** treated cells compared to control cells

Figure 6. **A.** Experimental procedure outline **B.** Number of differentially expressed genes (DEG) at 12 and 24 h in HeLa cells treated with **RuT$_7$** or CDDP compared to control. **C.** Venn diagrams representing specific and commonly deregulated genes (FDR<0.05 and FC>2) in HeLa cells at 12 and 24 h upon treatment with **RuT$_7$** (in red) and CDDP (in green)

Figure 7. Heatmap representing supervised hierarchical clustering over most variable (above mean standard deviation) significantly differentially expressed genes between **RuT$_7$** and control treated HeLa cells. **A)** at 12 h; **B)** at 24 h. Genes expressed above median are pseudo-colored in red, bellow median in green. **C)** Venn diagram showing specific and common differentially expressed genes in HeLa cells treated with **RuT$_7$** at 12 and 24 h.

Figure 8. Group plots show the direction of expression changes for each gene cluster over time (12 h and 24 h) measurements and the differences between the **RuT$_7$** (green) and control-treated cells (red). Genes are clustered by similar patterns and an average gene expression level is represented for each cluster, with associated 95% CI (upper and lower dots). The slope coefficient represents the values of the estimated regression coefficients, positive for induced gene clusters, negative for repressed gene clusters.

Figure 9. Bar chart depicting significantly enriched (FDR<0.05) toxicity functions determined by IPA Tox Comparison Analysis